Monograph:
Morris, A.S. and Madani, A. (1995) Static and Dynamic Modelling of a Two-Flexible-Link Robot Manipulator. Research Report. ACSE Research Report 586 . Department of Automatic Control and Systems Engineering

---

STATIC AND DYNAMIC MODELLING OF A TWO-FLEXIBLE-LINK ROBOT MANIPULATOR

A. S. MORRIS and A. MADANI

Robotics Research Group,
Department of Automatic Control and Systems Engineering,
The University of Sheffield, Mappin Street, Sheffield, S1 3JD, United Kingdom.

RESEARCH REPORT NUMBER 586
29 June 1995

STATIC AND DYNAMIC MODELLING OF A TWO-FLEXIBLE-LINK ROBOT MANIPULATOR

by

A. S. Morris, BEng, PhD, CEng, MIEE, MInstMC and A. Madani, BEng

Abstract—This paper is addressed at the difficulty of accurately modelling a two-flexible-link manipulator system, which is a necessary pre-requisite for future work developing a high-performance controller for such manipulators. Recent work concerned with the development of an accurate single-flexible-link model is first reviewed and then the expansion of a single-link model into a two-flexible-link system in a way which properly takes into account the coupling and interactions between the two links is discussed. The method of approach taken is to calculate the elastic and rigid motions of the links separately and then to combine these according to the principle of superposition. The application of the model developed is demonstrated in a simulated two-flexible-link system.

1 Introduction

The use of small section, low mass links in robot manipulators is attractive because it avoids the severe control problems associated with the large inertia forces generated when the large-mass links in a conventional manipulator move at anything other than low speed. Unfortunately, the control problem is not eliminated but only changed: instead of on-line compensation for inertia forces, the controller has to respond to link flexure and the consequent vibrations.

The necessary pre-requisite for a flexible manipulator controller is the existence of a suitably accurate model of the manipulator system. In practice, a typical revolute-geometry industrial robot manipulator has six degrees of freedom but the problematical inertia forces are due to just two of the links within it. Thus, it will normally only be necessary to have a manipulator with two flexible links to avoid large inertia forces and the ensuing control problems: all other links can remain rigid. Hence, the necessary manipulator model can be divided into two connected sub-systems: a two-flexible-link model and a model of the other rigid links.

The starting point in modelling a two-flexible-link system is a single-link model. Two such models can then be assembled together, but in a way which takes proper account of the coupling and interaction between the link motions. Because of this inter-link coupling, any modelling errors will be cumulative, and hence high accuracy is essential in the single-link model on which the two-link model is built.

Until a short time ago, a flexible-link model of adequate accuracy did not exist, but this problem has been now been redressed by recent work. This paper will start by summarising this recent development of an accurate single-flexible link model and will go on to explain the expansion of this into a two-flexible-link model which takes proper account of inter-link coupling.

2 Static Single-Link Model

The assumed mode method (AMM) is a computationally efficient scheme which serves as a useful starting point in formulating a flexible link model. Assuming the magnitude of flexure to be low, the slope and static deflection of a flexible beam bending under gravity are described by:

$$\frac{du_m}{dx} = -\frac{mg}{2EIl}\left(l^2x - lx^2 + \frac{x^3}{3}\right) \; ; \quad u_m = -\frac{mg}{2EIl}\left(\frac{l^2x^2}{2} - \frac{lx^3}{3} + \frac{x^4}{12}\right) \tag{1}$$

where m is the mass of the beam, l is the length of the beam, EI is the flexural stiffness of the beam, g is the gravity vector, x is the position on the beam of the point where the slope and deflection is measured and the subscript m denotes the slope or deflection resulting from the mass of the beam.

For a flexible link with an end-tip load m_t (Figure 1), the mass m_t produces a negative slope and deflection given by:

$$\frac{du_{m_t}}{dx} = -\frac{m_t g}{EI}\left(lx - \frac{x^2}{2}\right) \; ; \qquad u_{m_t} = -\frac{m_t g}{EI}\left(\frac{lx^2}{2} - \frac{x^3}{6}\right) \tag{2}$$

By the principle of superposition the total static slope and deflection for a flexible link are given by:

$$\frac{du}{dx} = \frac{du_m}{dx} + \frac{du_{m_t}}{dx} = -\frac{g}{2EIl}\left((m+2m_t)l^2x - (m+m_t)lx^2 + \frac{mx^3}{3}\right)$$

$$u = u_m + u_{m_t} = -\frac{g}{2EIl}\left((m+2m_t)\frac{l^2x^2}{2} - (m+m_t)\frac{lx^3}{3} + \frac{mx^4}{12}\right) \tag{3}$$

The maximum static slope and deflection of the flexible link occur at the free end, where $x = l$, i.e.

$$\frac{du_{max}}{dx} = -\frac{l^2 g}{2EI}\left(\frac{m}{3} + m_t\right) \; ; \qquad u_{max} = -\frac{l^3 g}{2EI}\left(\frac{m}{4} + \frac{2m_t}{3}\right) \tag{4}$$

The deflection of the link end-tip is calculated in the above equations on the assumption that the end-tip moves vertically downwards instead of in a circular arc. This is clearly only valid if the magnitude of flexure is low. This condition is unlikely to be satisfied in typical industrial flexible manipulator links, and modification of the equations is therefore necessary.

Previous work [1] has shown that the case of large magnitude flexure can be handled by adding a correction factor to the basic equations. This is calculated by considering the link as a body composed of n equal sections and applying finite element analysis.

The corrected coordinates of the end-tip are then given by [1]:

$$x_e = l - s \qquad \text{and} \qquad y_e = u(l-s) \tag{5}$$

where:

$$s = \sum_{i=1}^{n-1} w_i \tag{6}$$

$$v_n = L - l/n \; ; \qquad w_n = \frac{v_n l}{nL} \; ; \qquad L = \sqrt{\left(u(l-s) - u((n-1)l/n - s)\right)^2 + (l/n)^2} \tag{7}$$

$$u(l - s - w_n) = \frac{w_n}{v_n}\, u(l-s) \tag{8}$$

3 Dynamic Single-Link Model

The equation of motion of an undamped flexible link without payload is described by [2] and [3]:

$$\rho\frac{\partial^2 u(x,t)}{\partial t^2} = -\frac{\partial^2}{\partial x^2}\left(EI\frac{\partial^2 u(x,t)}{\partial x^2}\right) \; ; \qquad u(x,t) = \phi(x)q(t) \tag{9}$$

where ρ is the mass per unit length of the link, $u(x,t)$ is the deflection of the link, $\phi(x)$ is the assumed mode shape function and $q(t)$ is the modal function. Assuming that EI is a constant, allows Eq. (9) to be written as

$$\frac{1}{q(t)}\frac{d^2q(t)}{dt^2} = -\frac{EI}{\rho}\frac{1}{\phi(x)}\frac{d^4\phi(x)}{dx^4} \tag{10}$$

which leads to the two following differential equations:

$$\frac{d^4\phi(x)}{dx^4} - \beta^4\phi(x) = 0 \; ; \qquad \frac{d^2q(t)}{dt^2} + \omega^2 q(t) = 0 \tag{11}$$

where w is a constant and $\beta^4 = \rho\omega^2/EI$.
The solution as found in [2] and [3] is:

$$\phi_i(x) = C_i(\cos\beta_i x - \cosh\beta_i x) + (\sin\beta_i x - \sinh\beta_i x) \tag{12}$$

and

$$q_i(t) = A_i \cos\omega_i t + B_i \sin\omega_i t \tag{13}$$

where A_i, B_i, C_i and ω_i are constants, i denotes the number of modes of vibration. The deflection is then given by

$$u(x,t) = \sum_{i=1}^{\infty} \phi_i(x) q_i(t) \tag{14}$$

From the boundary conditions ($u(0,t) = u(l,t) = \frac{\partial u}{\partial x}(0,t) = \frac{\partial^2 u}{\partial x^2}(l,t) = 0$) we obtain

$$C_i = \frac{\cos\ \beta_i l + \cosh\ \beta_i l}{\sin\ \beta_i l - \sinh\ \beta_i l} \tag{15}$$

and β_i as a solution to

$$\cos\ \beta_i l\ \cosh\ \beta_i l = -1 \tag{16}$$

Solving Eq. (16) for the first four modes gives $\beta_1 l = 1.875$, $\beta_2 l = 4.694$, $\beta_3 l = 7.854$ and $\beta_4 l = 10.995$. From here, using the definition that $\beta_i^4 = \rho\omega_i^2/EI$, we can deduce the values of the natural frequencies ω_i of the flexible link for the first four modes. This means that, given an initial excitation F, the link is going to oscillate according to a combination of these four natural frequencies.

The equation of motion can be generalised as an eigenvalue problem linking the two parts of the system (the assumed mode shape functions $\phi_i(x)$ and the modal functions $q_i(t)$). Subsequent analysis [1] taking into account the first three modes (i =1,2 and 3) leads to the following equations for the vertical displacement $u(x,t)$ of any point x on the link at any time t, the slope $u'(x,t)$ of the link at any point x and any time t and the velocity $\dot{u}(x,t)$ of any point x on the link at any time t:

$$u(x,t) = \phi_1(x)q_1(0)\cos\omega_1 t + \phi_2(x)q_2(0)\cos\omega_2 t + \phi_3(x)q_3(0)\cos\omega_3 t \tag{17}$$

$$u'(x,t) = \frac{\partial u(x,t)}{\partial x} = \phi_1'(x)q_1(0)\cos\omega_1 t + \phi_2'(x)q_2(0)\cos\omega_2 t + \phi_3'(x)q_3(0)\cos\omega_3 t \tag{18}$$

$$\dot{u}(x,t) = \frac{\partial u(x,t)}{\partial t} = -\phi_1(x)q_1(0)\omega_1\sin\omega_1 t - \phi_2(x)q_2(0)\omega_2\sin\omega_2 t - \phi_3(x)q_3(0)\omega_3\sin\omega_3 t \tag{19}$$

subject to the initial conditions:

$$u(x,0) = \sum_{i=1}^{\infty}\phi_i(x)q_i(0) = f(x) \; ; \qquad \dot{u}(x,0) = \sum_{i=1}^{\infty}\phi_i(x)\dot{q}_i(0) = g(x) \tag{20}$$

Using the orthogonal relation, the corresponding initial conditions in the *normal coordinates* (the normalisation or weighting is operated on all modes) are

$$q_i(0) = \frac{\rho l}{m_{ii}}\int_0^l f(x)\phi_i(x)dx \; ; \qquad \dot{q}_i(0) = \frac{\rho l}{m_{ii}}\int_0^l g(x)\phi_i(x)dx \tag{21}$$

Similarly, $q_i(0)$ and $\dot{q}_i(0)$ can be obtained from the normalised flexural stiffness as

$$q_i(0) = \frac{EI}{k_{ii}}\int_0^l f''(x)\phi_i''(x)dx \; ; \qquad \dot{q}_i(0) = \frac{EI}{k_{ii}}\int_0^l g''(x)\phi_i''(x)dx \tag{22}$$

When an end-tip load is added to the link, an extra eigenvalue will appear in the boundary conditions and it can be shown [1] that the effect is to cause the link to vibrate at a slower frequency and for vibrations to persist for a longer period of time.

3.1 Shear Deformation Effect

The assumed mode method neglects shear deformation effects and calculates link deformation on the assumption that this is due only to the bending moment created by the mass and end-tip load of the link. This assumption appears to have been made in all flexible link models previously reported. However, a shear force also exists which acts in the opposite direction to the bending moment and produces motion which has been shown to be significant [4]. Thus, in the interests of accurate modelling, the shear deformation effect must be included in both static and dynamic models of a flexible link.

It is known that the shear force of flexible arms depends on the shape of the cross-section of the arm. Therefore, a physical quantity called the *numerical factor*, representing the geometric characteristics of the link cross-section, is required in the dynamic formulation of the manipulator.

Referring to [5], the numerical factor of a flexible beam is defined as

$$K = \frac{AQ}{I_a d} \tag{23}$$

where, I_a is the moment of inertia of the cross-sectional shape of the link computed with respect to its neutral axis, Q denotes the first moment about the neutral axis of the area contained between an edge of the cross-section of the beam parallel to the main axis and the surface at which the shear stress is to be computed, A is the cross-sectional area and d is the width of the cross-sectional area at which the shear deformation is required. For a uniform link of square cross section, the factor K is given by:

$$K = \frac{AQ}{I_a d} = \frac{d^2(\rho l)l^2/2}{(\rho l)l^2 d/3} = \frac{3d}{2} \tag{24}$$

An element dx of the flexible link is deformed by the shear force V and the bending moment M shown in Figure 2. When the shear force is zero, the centre line of dx is normal to the face of the cross-section. If $\partial u(x,t)/\partial x$ is the slope due to the bending moment M, neglecting the interaction between the shear and the moment, the shear force will cause a rectangular element to become a parallelogram without a rotation of the faces.

Thus, the slope of the deflection curve is decreased by the shear angle as formulated in the following equation:

$$\frac{\partial u_c(x,t)}{\partial x} = \frac{\partial u(x,t)}{\partial x} - \frac{V}{KAG} \tag{25}$$

where V is the value of the shear force and is equal to $EI\rho$, G the shear modulus of the material the link is made of and $\partial u_c/\partial x$ the total slope cause by both shear and moment.

As a result of the above formulation, the equation of motion of an undamped flexible link after addition of the shear deformation becomes

$$EI\frac{\partial^4 u_c}{\partial x^4} + \rho\frac{\partial^2 u_c}{\partial t^2} - \frac{EI\rho}{KAG}\frac{\partial^4 u_c}{\partial x^2 \partial t^2} = 0 \tag{26}$$

This equation is very difficult to solve because of the last term in the left hand-side. However, supposing that the shear force affects only the modal functions $q_i(t)$, a solution is found in [6] as being

$$\phi_i(x) = A_i(\cos\beta_i x - \cosh\beta_i x) + \sin\beta_i x - \sinh\beta_i x \tag{27}$$

and

$$q_{ci}(t) = q_{ci}(0)\cos(\omega_{ci}t + \psi) \tag{28}$$

where β_i are obtained in the same manner as for the system without shear deformation, (i.e., as in section 3) and ω_{ci} are the transformed natural frequencies including the shear deformation and are given by

$$\omega_{ci} \simeq \omega_i \left[1 - \frac{1}{2}\frac{EI}{KAG}\beta_i^2\right] \tag{29}$$

ω_i being the natural frequencies of the system without shear deformation.
The angle ψ is equal to

$$\psi = \frac{V}{KAG} = \frac{'EI\rho}{KAG} \tag{30}$$

From this set of equations, we can see how the shear deformation decreases the natural frequencies of vibration of the link. The effect is more pronounced for the higher modes because of the existence of the term β_i^2 in the equation for ω_{ci}. The total slope is also decreased by the amount ψ. Thus it is apparent that the shear deformation acts similarly to a load on the frequency of the system, but operates in the opposite manner for the slope.

4 Two-Flexible-Link Model

The main difficulty in modeling multi-link flexible manipulators is that the rigid motion and the elastic motion are coupled together, and the elastic motion has direct effects on the transformation matrix between the link coordinates and the global coordinates. Due to the complexity of the problem, the modeling of flexible manipulators is initially simplified by neglecting the effect of the elastic motion on the transformation matrix and neglecting the effect of the elastic motion on the rigid motion.

If the rigid motion is not affected by the elastic motion, the rigid system dynamic equations can be derived using the Lagrange-Euler principle. These equations can then be used to predict the dynamic stress and elastic deformation of the system, by applying the respective torques obtained for the rigid motion to the dynamic equations describing the elastic motion. For the two-link flexible case, this is difficult because of the cross-interaction between the two links, which consists of:

1. Action of the second link on the first link. This effect is created by any type of motion of the second link (rotary, vibrational or both), causing the first link to vibrate according to its natural frequencies.

2. Action of the first link on the second link. This effect is created by any type of motion of the first link (rotary, vibrational or both) causing the second link to move in a highly nonlinear manner.

The task of modeling a two-link flexible manipulator is made even harder by the fact that this cross-interaction between the two links is permanently present, i.e., a small disturbance at the end-tip of the first link will cause this link to start a vibrational motion, causing the second link to engage in a motion that will affect the vibrational motion of the first link, and so on ...

To avoid this problem and simplify the modeling of a two-link flexible manipulator without compromising on accuracy, the first type of cross-interaction will be ignored, by assuming that any energy produced in the second link is absorbed through the actuator of this link and therefore cannot propagate to the first link. Thus, the following modelling methodology can be applied:

1. Define the equations of motion for the rigid motion by formulating the necessary torques that are going to be applied to the respective actuators either by choosing the appropriate angles of rotation θ_i, or by using the initial cartesian and desired cartesian coordinates of the manipulator.

2. Define the set of dynamic equations for the flexible motion (only the flexible modes are included in this formulation). From here, a state-space representation of the flexible system can be sought in order to study the elastic behaviour of each link.

3. Apply the desired torques to the flexible system.

4. Implement the Correction Factor in the response.

5. Combine the two motions (rigid and elastic) according to the principle of superposition and deducing the general motion of the manipulator.

This modelling methodology for the elastic motion has been further simplified by the use of only the first three flexible modes, since higher modes have negligible influence on the behaviour of the system [1] and [4].

4.1 Rigid Motion

The rigid motion of a two-link manipulator can be described in terms of the Lagrange-Euler formulation:

$$\frac{d}{dt}\left[\frac{\partial L}{\partial \dot{\theta}_i}\right] - \frac{\partial L}{\partial \theta_i} = \tau_i \qquad i = 1, 2. \tag{31}$$

where L is the Lagrangian function and is equal to $K - P$, K is the total kinetic energy of the robot arm, P is the total potential energy of the robot arm, θ_i are the angular joint positions, τ_i are the generalised torques applied to the system at joint i to drive link i as defined in:

$$\tau_i = \sum_{k=1}^{n} D_{ik}\ddot{\theta}_k + \sum_{k=1}^{n}\sum_{m=1}^{n} h_{ikm}\dot{\theta}_k\dot{\theta}_m + c_i \qquad i = 1, 2. \tag{32}$$

or in a matrix form as

$$\tau(t) = D(\theta(t))\ \ddot{\theta}(t) \ + \ h(\theta(t), \dot{\theta}(t)) \ + \ c(\theta(t)) \tag{33}$$

where $\tau(t)$ is a 2×1 generalised torque vector applied at joints $i = 1, 2$.
$\theta(t)$ is a 2×1 vector of the joint positions,
$\dot{\theta}(t)$ is a 2×1 vector of the joint velocities,
$\ddot{\theta}(t)$ is a 2×1 vector of the joint accelerations,
$D(\theta)$ is a 2×2 inertial acceleration-related symmetric matrix whose elements were calculated in [7] as:

$$\begin{aligned} D_{11} &= \frac{2/3m_1^2l^2 + 2/5m_m^2d_m^2 + m_1m_m(4/3l^2 + 4/5d_m^2)}{(2m_1 + m_m)} \\ &+ \frac{m_2^2(8/3l^2 + 2l^2\cos\theta_2) + m_t^2(l^2 + 2/5d_t^2)}{(2m_2 + m_t)} \\ &+ \frac{m_2m_t(13/3l^2 + l^2\cos\theta_2 + 4/5d_t^2)}{(2m_2 + m_t)} \end{aligned} \tag{34}$$

$$D_{12} = D_{21} = \frac{m_2^2l^2(2/3 + \cos\theta_2) + 2/5m_t^2d_t^2 + m_2m_t(4/3l^2 + l^2\cos\theta_2 + 4/5d_t^2)}{(2m_2 + m_t)} \tag{35}$$

and

$$D_{22} = \frac{2/3m_2^2l^2 + 2/5m_t^2d_t^2 + m_2m_t(4/3l^2 + 4/5d_t^2)}{(2m_2 + m_t)} \tag{36}$$

where m_1 and m_2 are the masses of the first and second links respectively, m_m is the mass of the actuator located at the end-tip of the first link, m_t is the mass of the load at the end-tip of the second link, d_m is the radius of the actuator (considered to be spherical), and d_t is the radius of the load (also considered to be spherical).
$h(\theta, \dot{\theta})$ is a 2×1 nonlinear Coriolis and centrifugal force vector given by

$$h(\theta, \dot{\theta}) = \begin{bmatrix} -\frac{m_2(m_2+m_t)l^2\sin\theta_2}{(2m_2+m_t)}\ (\dot{\theta}_2^2 + 2\dot{\theta}_1\dot{\theta}_2) \\ \frac{m_2(m_2+m_t)l^2\sin\theta_2}{(2m_2+m_t)}\ \dot{\theta}_1^2 \end{bmatrix} \tag{37}$$

and finally $c(\theta)$ is a 2×1 gravity loading force vector given by

$$c(\theta) = \begin{bmatrix} gl\left(\frac{m_1(m_1+m_m)}{(2m_1+m_m)}\cos\theta_1 + \frac{m_2(m_2+m_t)}{(2m_2+m_t)}\cos(\theta_1+\theta_2) + (m_2+m_t)\cos\theta_1\right) \\ -gl\frac{m_2(m_2+m_t)}{(2m_2+m_t)}\cos(\theta_1+\theta_2) \end{bmatrix} \tag{38}$$

4.2 Work Space

For a two-link rigid manipulator operating in the vertical plane, the work space is a circle of radius equal to the sum of the lengths of the two rigid links (see Figure 3). If the links are flexible, the radius of the circle is reduced by link flexure and becomes a function of the length, width, stiffness, mass and loading of each link. To determine the value of the radius of the circle of influence of a two-link flexible manipulator, it is necessary to first determine the static deflections at the end-tip of each of the links, then obtain the value of the horizontal deformations associated with these deflections. The static deflection at the end-tip of the second link is given by

$$u_2(l) = -\frac{l^3 g}{2EI}\left(\frac{m_2}{4} + \frac{2m_t}{3}\right) \tag{39}$$

where m_2 is the mass of the second link and m_t is the mass of the payload.
The static deflection at the end-tip of the first link is given by

$$u_1(l) = -\frac{l^3 g}{2EI}\left(\frac{m_1}{4} + \frac{2(m_t+m_2+m_m)}{3}\right) \tag{40}$$

where m_1 is the mass of the first link and m_m is the mass of the actuator for the second link considered to be a part of the payload for the first link. The two links are considered to have the same length l and the same stiffness EI.

Using the correction factor discussed in section 2, the static deflections at both end-tips are corrected and the horizontal projections (L_1' and L_2') of the deformed links are calculated. The maximum reach (L_i) for each link is deduced from the following equation:

$$L_i = \sqrt{(L_i')^2 + (u_{ic}(l))^2} \qquad i = 1, 2. \tag{41}$$

where the subscript c denotes that the correction factor has been applied to the variable. The radius of the circle of influence of a two-link flexible manipulator is therefore

$$R = L_1 + L_2 \tag{42}$$

4.3 State-Space Representation of the Flexible System

It was shown in [1], [2] and [3] that, the equation of elastic motion of a flexible link which is part of a multi-link system can be written as:

$$u_j(x,t) = \sum_{i=1}^{n} \phi_{ij}(x) q_{ij}(t) \tag{43}$$

where the subscript j denotes the link number ($j = 1$ for the first link),the subscript i denotes the mode number, $u_j(x,t)$ is the vertical deflection of the link j at the distance x and time t, $\phi_{ij}(x)$ is a shape function defined in [2] and [3], and $q_{ij}(t)$ is a modal function solution of the following second order differential equation:

$$\frac{d^2 q_{ij}(t)}{dt^2} + \frac{c_j}{m_{ij}}\frac{dq_{ij}(t)}{dt} + \omega_{ij}^2 q_{ij}(t) = \tau_j(t) \tag{44}$$

where c_j is the damping coefficient of the link, m_{ij} is the normalised mass for each mode i of the link j and ω_{ij} is the corresponding frequency equal to $\sqrt{k_{ij}/m_{ij}}$, k_{ij} being the normalised stiffness of the ith mode of the jth link.

Typically, the contributions of the flexible modes attenuate rapidly with frequency such that it is always possible to characterise the system dynamics to any required degree of accuracy with only a finite number of the lower modes. Bhat and Miu [8] and Korolov and Chen [9] have formulated a state-space representation for a one-link flexible manipulator by including the rigid mode in the matrix representation. This is valid only when the deflections or the vibrations of the flexible link are very small (slopes of less than 10 degrees), otherwise, the rigid motion of the deformed link becomes inappropriate and the state-space representation becomes inevitably inaccurate. For this reason, the flexible system is first studied separately from the rigid system, then, the various flexible variables such as end-tip deflection, end-tip slope, etc., are corrected. Finally, the two motions are combined to describe the whole system.

Considering only the first three flexible modes of each link, the flexible system can be described in the following state variable form:

$$\begin{Bmatrix} \dot{q}_{1j} \\ \ddot{q}_{1j} \\ \dot{q}_{2j} \\ \ddot{q}_{2j} \\ \dot{q}_{3j} \\ \ddot{q}_{3j} \end{Bmatrix} = \begin{bmatrix} 0 & 1 & 0 & 0 & 0 & 0 \\ -\omega_{1j}^2 & -\frac{c_j}{m_{1j}} & 0 & 0 & 0 & 0 \\ 0 & 0 & 0 & 1 & 0 & 0 \\ 0 & 0 & -\omega_{2j}^2 & -\frac{c_j}{m_{2j}} & 0 & 0 \\ 0 & 0 & 0 & 0 & 0 & 1 \\ 0 & 0 & 0 & 0 & -\omega_{3j}^2 & -\frac{c_j}{m_{3j}} \end{bmatrix} \begin{Bmatrix} q_{1j} \\ \dot{q}_{1j} \\ q_{2j} \\ \dot{q}_{2j} \\ q_{3j} \\ \dot{q}_{3j} \end{Bmatrix} + \begin{bmatrix} 0 \\ b_{1j} \\ 0 \\ b_{2j} \\ 0 \\ b_{3j} \end{bmatrix} \tau_j(t)$$

and with the position vector given by:

$$u_j(x,t) = [\phi_{1j}(x)\ 0\ \phi_{2j}(x)\ 0\ \phi_{3j}(x)\ 0][q_{1j}\ \dot{q}_{1j}\ q_{2j}\ \dot{q}_{2j}\ q_{3j}\ \dot{q}_{3j}]^T \tag{45}$$

This description can also be expressed in the following simplified form:

$$\begin{cases} \dot{q}_j = A_j\ q_j + B_j\ \tau_j \\ u_j(x) = C_j(x)\ q_j \end{cases} \tag{46}$$

The constants b_{ij} are obtained after normalisation of the torques τ_j for each mode of the flexible link j. The state-space representation given by Eqs. (45) is incomplete without the initial conditions relating to each link such as static deflection, relative position of each link in the reference frame and effect of the first link on the second link. These points will be discussed in the next sections by studying each link separately.

4.3.1 Link 1

According to Eqs. (45), the elastic motion of the first flexible link can be described by the following state-space representation:

$$\begin{Bmatrix} \dot{q}_{11} \\ \ddot{q}_{11} \\ \dot{q}_{21} \\ \ddot{q}_{21} \\ \dot{q}_{31} \\ \ddot{q}_{31} \end{Bmatrix} = \begin{bmatrix} 0 & 1 & 0 & 0 & 0 & 0 \\ -\omega_{11}^2 & -\frac{c_1}{m_{11}} & 0 & 0 & 0 & 0 \\ 0 & 0 & 0 & 1 & 0 & 0 \\ 0 & 0 & -\omega_{21}^2 & -\frac{c_1}{m_{21}} & 0 & 0 \\ 0 & 0 & 0 & 0 & 0 & 1 \\ 0 & 0 & 0 & 0 & -\omega_{31}^2 & -\frac{c_1}{m_{31}} \end{bmatrix} \begin{Bmatrix} q_{11} \\ \dot{q}_{11} \\ q_{21} \\ \dot{q}_{21} \\ q_{31} \\ \dot{q}_{31} \end{Bmatrix} + \begin{bmatrix} 0 \\ b_{11} \\ 0 \\ b_{21} \\ 0 \\ b_{31} \end{bmatrix} \tau_1(t)$$

where

$$m_{i1} = \int_0^l [\rho + m_l \delta(x-l)]\phi_{i1}^2 dx \qquad i = 1,2,3. \tag{47}$$

m_l being the mass of the payload for the first link which consists of the mass m_a of the actuator of the second link, the mass ρl of the second link and the mass m_t of the payload at the end-tip of the

second link.

The normalised flexural stiffness k_{i1} relative to each mode is given by

$$k_{i1} = \int_0^l EI(\phi_{i1}'')^2 dx \qquad i = 1, 2, 3. \tag{48}$$

The constants b_{i1} are deduced from the normalisation of the principal torque $\tau_1(t)$ applied to the link, and are equal to

$$b_{i1} = -\frac{\phi_{i1}(l)}{k_{i1}} \tag{49}$$

The position vector giving the deflection of the link at any point x is

$$u_1(x,t) = [\phi_{11}(x)\ 0\ \phi_{21}(x)\ 0\ \phi_{31}(x)\ 0][q_{11}\ \dot{q}_{11}\ q_{21}\ \dot{q}_{21}\ q_{31}\ \dot{q}_{31}]^T$$

This vector is increased by a value $u_{01}(x)$ corresponding to the static deflection caused by the mass of the link itself and the load attached to its end-tip. So, the deflection vector becomes:

$$u_1(x,t) = [\phi_{11}(x)\ 0\ \phi_{21}(x)\ 0\ \phi_{31}(x)\ 0][q_{11}\ \dot{q}_{11}\ q_{21}\ \dot{q}_{21}\ q_{31}\ \dot{q}_{31}]^T + u_{01}(x) \tag{50}$$

with

$$u_{01}(x) = -\frac{g}{2EIl}\left((\rho l + 2m_l)\frac{l^2x^2}{2} - (\rho l + m_l)\frac{lx^3}{3} + \frac{\rho l x^4}{12}\right) \tag{51}$$

The motion of the first link can be obtained from the inverse Laplace transform of the following equation:

$$u_1(x,s) = C_1(x)(sI - A_1)^{-1}B_1\ \tau_1(s) + u_{01}(x) \tag{52}$$

where s is the Laplace operator and I the identity matrix.

To determine the deflection u_1 at the end-tip of the first link, the variable x is replaced in Eq. (52) by l. Figure 4 shows the time history of this end-tip deflection for an impulse input of 1 Newton. The mass of both links is 400 grammes, the mass of the actuator for the second link is 200 grammes and the mass of the end-tip load of the second link is also 200 grammes.

The limitation of this state-space representation is that the response $u_1(x,t)$ will be relatively correct only for very small deflections. Since a good accuracy in determining the position of the end-tip of the first link is needed to locate the origin of the second link, the necessity in using the correction factor arises once again. The difficulty in using the correction factor lays in the fact that, unlike the normal procedure required by the state-space representation where the variable x is replaced by the value at which the deflection of the link is wanted (for this case x=l), the Correction Factor Method requires the value of the deflection all along the link. In order to obtain a good accuracy, the incrementation of the variable x has to be very small (independently from the number of finite elements chosen to approximate the flexible link). All this generates some extensive calculation and increases the computing time needed to obtain a response for the corrected deflection.

Figure 4 shows that, after applying the correction method to the deflection of the first link, the values obtained are smaller than those resulting from the solution of the Laplace transfer function relative to the first link. This, of course, will provide an acceptable basis for calculating the position of the second link and its general motion relatively to the first link.

A set of input torques (numbered 1 to 11) consisting of two consecutive impulses was applied to the actuator of the first flexible link (see Figure 5) to study the respective response of the end-tip deflection. These torques are not deduced from Eq. (33) and therefore do not result in any rotational motion. The link is only subject to a forced vibration due to the application of this set of torques.It can be seen from Figure 5(a) that the ideal torque would be torque number 5, since the forced vibration of the end-tip is successfully damped by the second impulse of this torque. It is also be observed that the forced vibration can be stopped by applying an impulse in the same direction as the initial impulse but after a delay determined by the frequency of the forced vibration, i.e. the second impulse should be generated during the second half-period of the first oscillation, or any consecutive second half-period.

4.3.2 Link 2

In the same manner as for the first link, the equations governing the elastic motion of the second link can be structured in a state-space representation as:

$$\begin{Bmatrix} \dot{q}_{12} \\ \ddot{q}_{12} \\ \dot{q}_{22} \\ \ddot{q}_{22} \\ \dot{q}_{32} \\ \ddot{q}_{32} \end{Bmatrix} = \begin{bmatrix} 0 & 1 & 0 & 0 & 0 & 0 \\ -\omega_{12}^2 & -\frac{c_2}{m_{12}} & 0 & 0 & 0 & 0 \\ 0 & 0 & 0 & 1 & 0 & 0 \\ 0 & 0 & -\omega_{22}^2 & -\frac{c_2}{m_{22}} & 0 & 0 \\ 0 & 0 & 0 & 0 & 0 & 1 \\ 0 & 0 & 0 & 0 & -\omega_{32}^2 & -\frac{c_2}{m_{32}} \end{bmatrix} \begin{Bmatrix} q_{12} \\ \dot{q}_{12} \\ q_{22} \\ \dot{q}_{22} \\ q_{32} \\ \dot{q}_{32} \end{Bmatrix} + \begin{bmatrix} 0 \\ b_{12} \\ 0 \\ b_{22} \\ 0 \\ b_{32} \end{bmatrix} \tau_2(t)$$

All the constants are determined in the same manner as for the first link.
The position vector giving the deflection at any point x on the link is:

$$u_2(x,t) = [\phi_{12}(x)\ 0\ \phi_{22}(x)\ 0\ \phi_{32}(x)\ 0][q_{12}\ \dot{q}_{12}\ q_{22}\ \dot{q}_{22}\ q_{32}\ \dot{q}_{32}]^T + u_{02}(x) \tag{53}$$

with $u_{02}(x)$ being the value of the static deflection of the link at a distance x from its origin. This static deflection is caused by the mass ρl of the link plus its payload m_t and is equal to

$$u_{02}(x) = -\frac{g}{2EIl}\left((\rho l + 2m_t)\frac{l^2x^2}{2} - (\rho l + m_t)\frac{lx^3}{3} + \frac{\rho l x^4}{12}\right) \tag{54}$$

In a similar manner to that of the first link, the response of the second link can be obtained from the inverse Laplace transform of the following equation:

$$u_2(x,s) = C_2(x)(sI - A_2)^{-1}B_2\ (\tau_1(s) + \tau_2(s)) + u_{02}(x) \tag{55}$$

Figure 6 shows the time history of the uncorrected, then corrected end-tip deflection for an impulse input of 1 Newton generated by the actuator of the second link only ($\tau_2(t)$= 0). It can be observed that the time needed by the link to regain its steady-state position is shorter (by almost 3 seconds) compared with that needed by the first link. This is due to the distribution of masses for the two links.

Figure 7 shows the effect of a set of input torques (generated in the same manner as for the first link) on the behaviour of the end-tip of the second link. The dynamic properties of the second link not being the same as those of the first link, the response of the corresponding end-tips is therefore totally different. For this case, the ideal torque is found to be torque number 9. The overshoot is minimum and the settling time, compared with the rest of the responses, faster.

The next step in the modeling of a two-link flexible manipulator consists of repositioning the origin of the second link. This is done by obtaining the corrected horizontal and vertical positions of the end-tip of the first link and assigning these values to the coordinates of the origin of the second link. Then, the vibration and (or) rotation of the first link is used as an additional input to the second link. This is considered as the effect of the first link on the second link. This operation is carried out by obtaining the time-varying slope $du_1(l,t)/dx$ of the end-tip of the first link through the correction factor method and adding it to the angular position $\theta_2(t)$ of the second link.

4.4 Final Model

The block diagram in Figure 8 summarises the modelling algorithm for the two-link flexible manipulator. The model is divided into two sub-systems, one for each link. Desired coordinates (x_{1d}, y_{1d}, x_{2d} and y_{2d}) are fed into the system through the block representing the inverse kinematics of the system to generate the desired angles of rotation $\theta_{1d}(t)$ and $\theta_{2d}(t)$. This operation can be omitted if these two desired angles are known initially. Both angles are then used as inputs for the rigid system models representing the two links. Outputs such as link masses, actuator mass, payload, stiffness, length and width of each link, etc., are passed to the second part of each sub-system which computes the elastic

motion of each link. Other important outputs produced by each of the two rigid model sub-systems are the applied torques $\tau_1(t)$ and $\tau_2(t)$. Each torque induces the corresponding rigid body to rotate according to the corresponding angle of rotation $\theta_d(t)$ and, simultaneously, provokes a forced vibration into the corresponding flexible sub-system.

The superposition of both motions (rigid and flexible) produces a set of variables for each link; among these are the end-tip vertical positions, the end-tip horizontal positions, the end-tip deflections and the end-tip slopes. Using the Correction Factor Method, all of these outputs are recalculated. As a result, some of them will be used as a feed-back to the whole system to test if the rotations are accomplished, while others (the end-tip slope of link 1, for instance) will be added to the angular position of the rigid body of the second link, therefore quantifying the effect that the first link has on the second link. To illustrate the mode of operation of the modeling algorithm, a simulation was carried out in which a rotation of +30 degrees was applied to the first link, while a rotation of -30 degrees was applied to the second link. As initial conditions (see Figure 9), the rigid body of the first link was taken to be horizontal ($\alpha_1 = 0$). This implies that the end-tip of the actual link is below the horizontal axis OX since the link is deflected by its loading and the loading of the second link. The second link was initially aligned with the first link ($\alpha_2 = 0$) meaning that the rigid body of link 2 is aligned with the tangent to the first link at its end-tip. A Correction Factor calculated using 6 finite elements for each link was used in obtaining the following results from the simulation.

Figure 10(a) shows the variation with time of the angle of rotation $\theta_1(t)$ of link 1. This angle (plus the variation of the angle of rotation of link 2) will be produced by applying a torque $\tau_1(t)$ (Eq. (33) to the actuator of link 1. This torque is shown in Figure 10(b). A nominal value of 4.8 Newtons is necessary to compensate for the gravity force, and should be applied to the actuator as long as the manipulator is in use.

It can be seen that the torque provokes first an acceleration (part of the curve which is above 4.8 Newtons), then a deceleration (part of the curve which is below 4.8 Newtons). The magnitude of these two variations depends mainly on the time necessary to rotate the link(s). For a faster time of rotation, the magnitude of the acceleration and deceleration torques is increased, and vice-versa.

Figure 10(c) shows how the end-tip deflection of the first link reacts to the variation of the torque. First, there is an increase in negative deflection (the link is starting to rotate, so the torque adds to the gravitational effect). After 0.15 seconds, the torque is decreased. This causes the link to try to regain its static equilibrium position (the value of the end-tip deflection jumps from -0.41 metres to -0.36 metres), but soon after, the torque is decreased even further (braking phase) causing a gradual overshoot for the end-tip deflection. In this phase, the deflection is decreased until the braking process has completely ceased. The link will then start oscillating according to its natural frequencies for the period of time determined by its damping coefficient.

To exactly clarify what is happening at the end-tip of the first link, a plot for the horizontal and vertical positions of this end-tip is shown in Figure 11. It can be seen that the initial coordinates for the position of the end-tip of the first link are (0.9,-0.34). After 5 seconds, the new position is given by the following coordinates (0.97,0.16) showing that the first link has rotated by 30.062 degrees (this value will equal 30 degrees as soon as the vibrations disappear).

A two-dimensional side view of the rotating first link is shown in Figure 12(a). The use of six finite elements to model the link achieves an accurate representation of the curvature. It can be noticed that the curvature (slope) is more pronounced towards the origin of the link (where the loading stress is maximum). The link is less curved towards its end-tip (where the loading stress is minimum). It can also be seen from this side view how the end-tip is pushed downwards at the beginning of the rotation. This is due to the fact that while the origin of the link is rotated upwards, the torque increase provokes the link to bend more and at the same time its inertia is trying to keep it at its initial position. The resulting effect is that the end-tip is brought downwards and towards the vertical axis for a very short period of time. When the link reaches the desired position (here, a vertical rotation of 30 degrees), the actuator is stopped and only the free damped vibrations of the link will remain. Figure 12(b) shows the same link under the same circumstances as Figure 12(a), but with an extra

dimension added to show the time history of the flexible link when rotating.

While the first link is being rotated upwards, the second link engages in a similar angular rotation but in the opposite direction. Fig. 6-13(a) shows the value of the angle of rotation $\theta_2(t)$. This angle is used in combination with the angle $\theta_1(t)$ to help determine the value of the torque $\tau_2(t)$ (see Eq. (33)) to be applied to the actuator of the second link.

Since the rotation is opposite to that of the first link, and since the loading involved in this motion is smaller than that involved with the first link, the resulting torque (Figure 13(a)) is found to be of a lesser magnitude than $\tau_1(t)$, causing the end-tip deflection (Figure 13(c)) to be smaller than its counterpart of link 1. The response of the end-tip deflection for the second link is exactly the opposite of the end-tip deflection of the first link, such that it is first decreased from its static equilibrium value since the link is starting to rotate downwards. This is followed by a phase of readjusting (the link tries to regain its static equilibrium deflection) and that is soon followed by the braking phase where the deflection is increased to a maximal negative value. Finally, the link is left to vibrate at its natural damped frequencies.

Figures 14(a) and (b) show the variation with time of the coordinates of the end-tip of the second link. These coordinates are expressed in the reference frame attached to the second link, and do not show the effect that the rotation of the first link has on the second link. In a similar manner to that of the first link, the angle of rotation of the second link can be derived by calculating the angle given at any time by the coordinates shown in Figure 14 and substracting this from the initial angle given by the coordinates at time zero.

The next step is to convert all the coordinates of all the points on the second link plus the corresponding deflections and slopes from the second link reference frame to the first link reference frame. By doing this, the effect of the first link on the second link is introduced. The value of the slope at the end-tip of the first link will act as an additional input to the second link. This will define the new motion of the second link. As a result, the new coordinates of the end-tip position of the second link are given in Figures 15(a) and (b). The vibrations caused by the action of the first link on the second link are magnified to a point where the second link's own vibrations are almost entirely absorbed by those of the first link.

Figures 16(a) and (b) show a two-dimensional and three-dimensional view of the motion of the two-link flexible manipulator. Since the two links rotate by the same angle but in opposite directions, the second link will tend to keep a position parallel to its initial position. This type of motion for the second link is valid only when $\theta_1(t)=-\theta_2(t)$.

5 Summary

In this paper, the accurate modelling of a two-link flexible manipulator has been studied. Based on the Lagrange-Euler formulation, the equations for calculating the necessary torques to be generated by the corresponding actuators to provoke the desired rotations $\theta_1(t)$ and $\theta_2(t)$ have been presented. The work space of the manipulator has also been considered and it has been shown that the reach is shortened due to its flexibility.

The approach to the development of a state-space representation of the two-link flexible system has been to consider the manipulator as two systems which are each divided into two sub-systems: a rigid sub-system and a flexible sub-system. The model has been used to study the time response of the deflection at the end-tip of link 1 and link 2 to an impulse input applied to each actuator was obtained. Initially, no correction was applied, and then the correction factor explained in section 2 was included in the model. This demonstrated that the modelling of flexible manipulators can be highly inaccurate

if this correction method is not applied. Finally, simulation of the behaviour of the two-link flexible manipulator model when the two joints are driven through certain angles was performed.

References

[1] Morris, A.S. and Madani, A, 1995, "Multi-Mode Modelling of a Flexible Link Robot Manipulator", Submitted for publication in Proceedings of the Inst. of Mech. Eng., Part I.

[2] Timoshenko, S., Young, D.H. and Weaver, W.Jr., 1974, *Vibration Problems in Engineering*. Wiley. New York.

[3] Cannon, R.H.Jr. and Schmitz, E., 1984, "Initial Experiments on the End-Point Control of a Flexible One-Link Robot", *Int. J. Robotics Res.*, Vol. 3, no. 3, pp. 62-75.

[4] Morris, A.S. and Madani, A, 1995, "Inclusion of Shear Deformation Term to Improve Accuracy in Flexible-Link Robot Modelling", Submitted for publication in *Mechatronics*

[5] Timoshenko, S. and Lessels, J.M., 1925, *Applied Elasticity*, First edition, Westinghouse Technical Night School Press.

[6] Tse, F.S., Morse, I.E. and Hinkle, R.T., 1978, "Mechanical Vibrations, Theory and Application", Second edition, Allyn and Bacon, Boston.

[7] Fu, K.S., Gonzalez, R.C. and Lee, C.S.G., 1987, *Robotics: Control, Sensing, Vision, and Intelligence*, Mc Graw-Hill International Edition.

[8] Bhat, S.P. and Mui, D.K., 1990, "Precise Point-to-Point Positioning Control of Flexible Structures", *Trans. ASME, Journal of Dynamic Systems, Measurement, and Control*, Vol. 112, pp. 667-674.

[9] Korolov, V.V. and Chen, Y.H., 1989, "Controller Design Robust to Frequency Variation in a One-Link Flexible Robot Arm", *Journal of Dynamic Systems, Measurement, and Control*, Vol. 111, pp. 9-14.

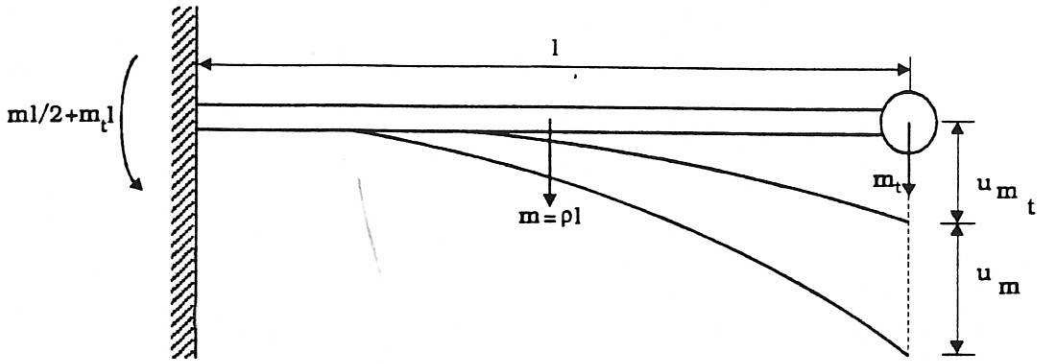

Figure 1. Deflection of a flexible link under the effect of its mass and payload.

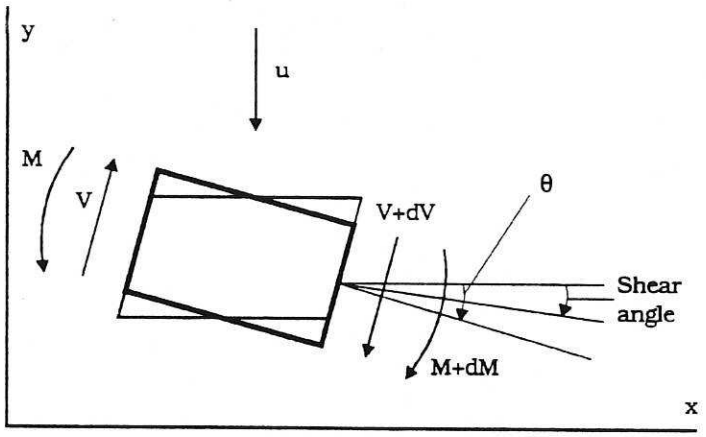

Figure 2. Lateral vibration of a beam with rotary inertia and shear deformation.

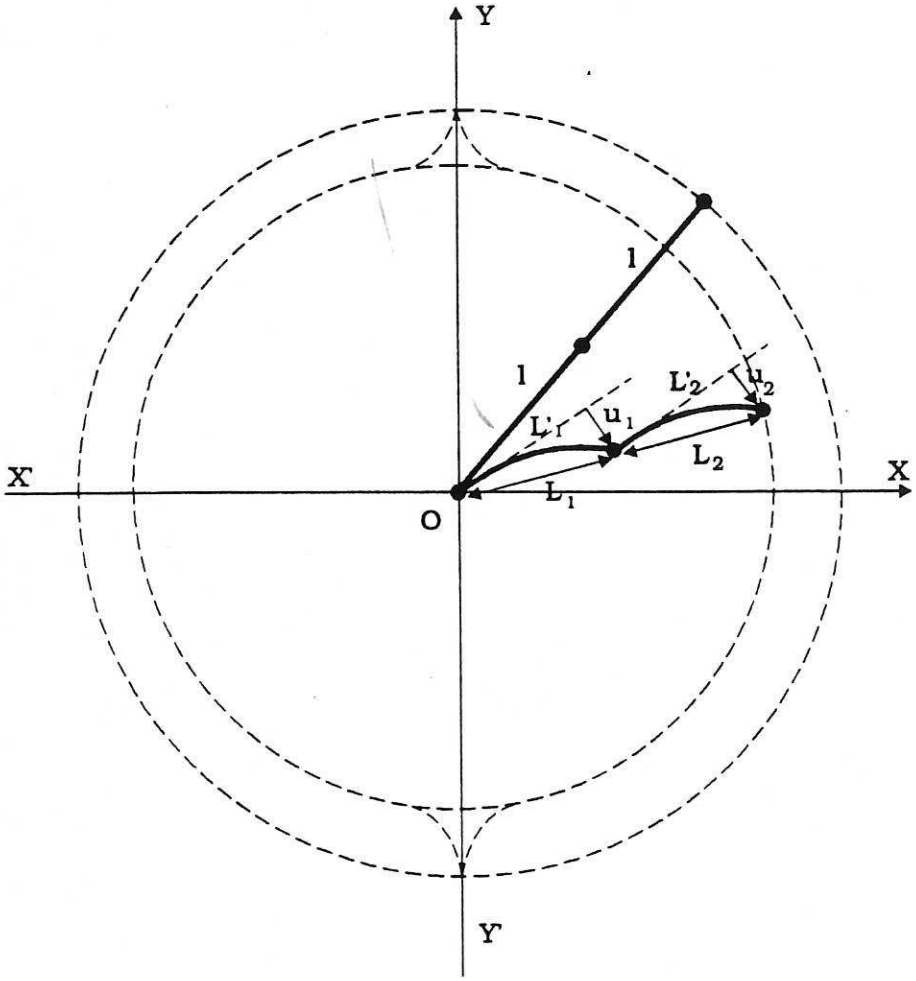

Figure 3. Work spaces for rigid and flexible manipulators.

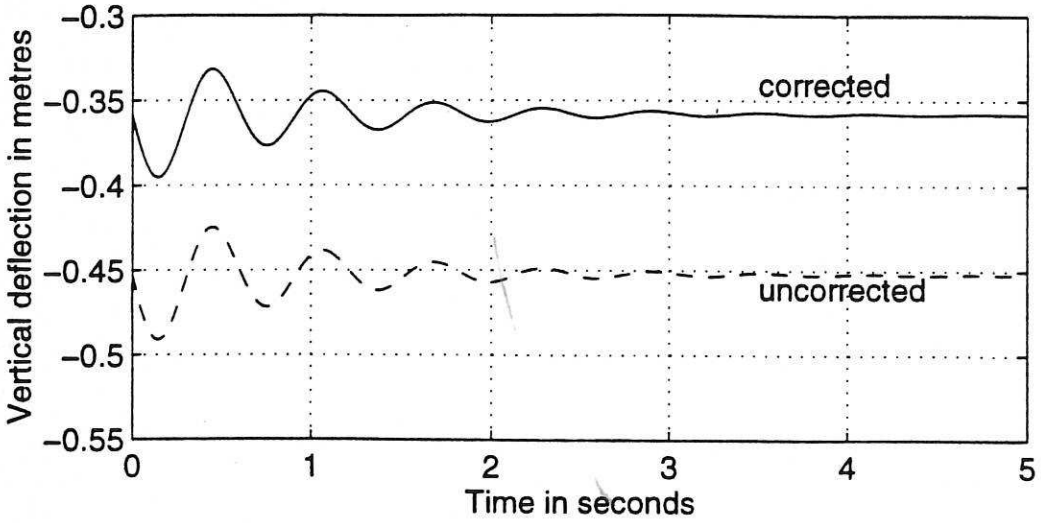

Figure 4. Response of the end–tip deflection of link 1
to an impulse input of 1 Newton.

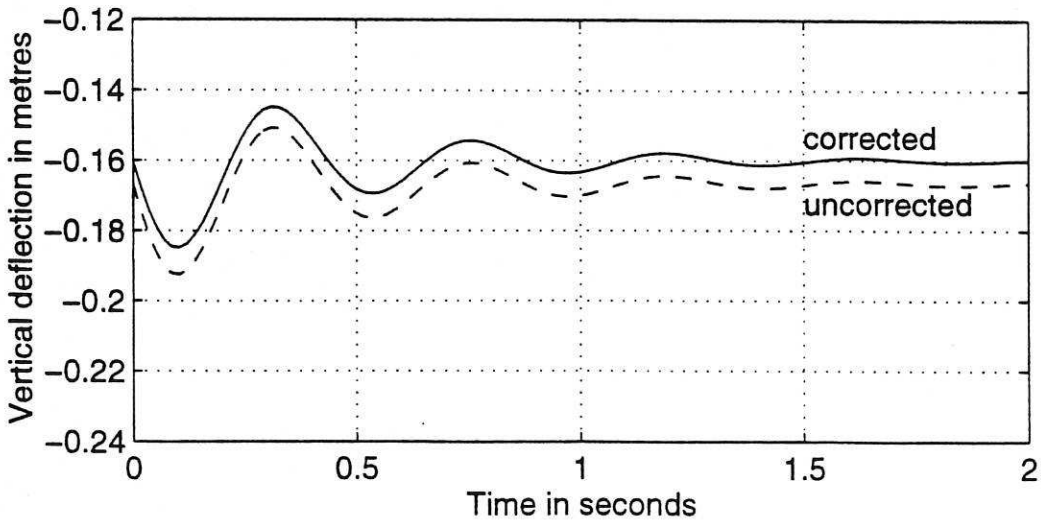

Figure 6. Response of the end–tip deflection of link 2
to an impulse input of 1 Newton.

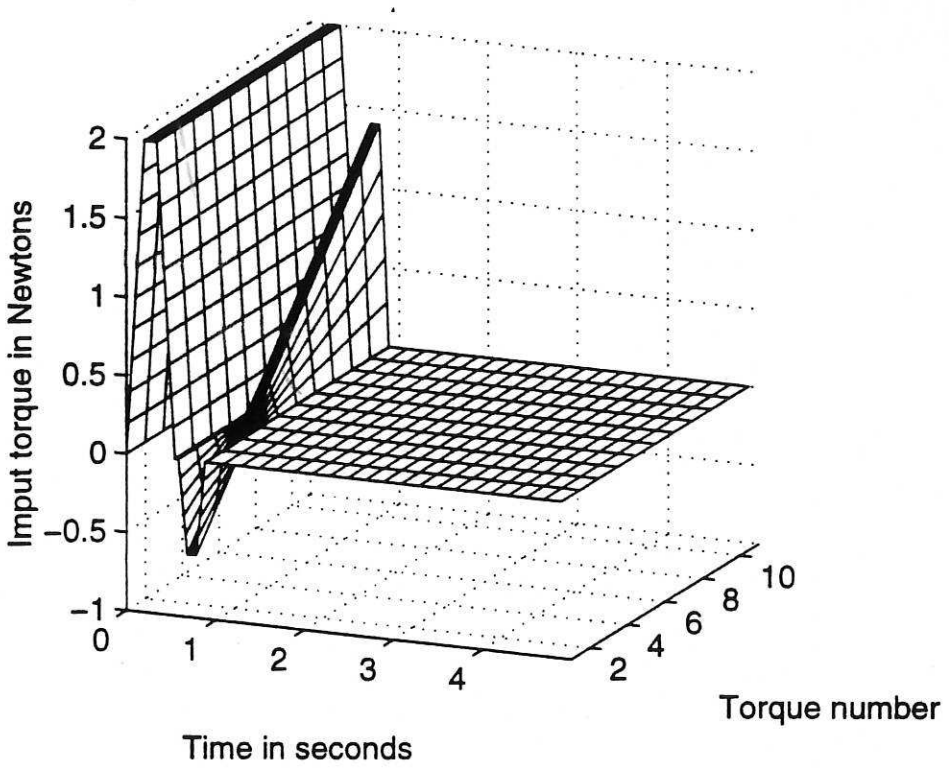

Figure 5(a). Input torque for the first link.

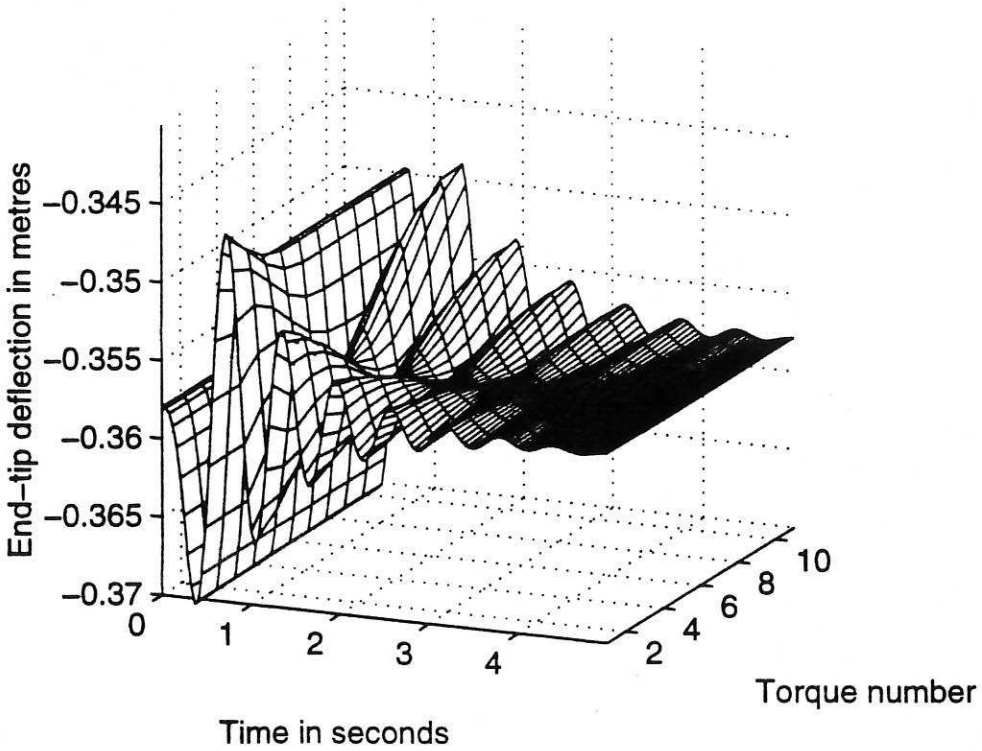

Figure 5(b). Response of the end−tip deflection of link 1.

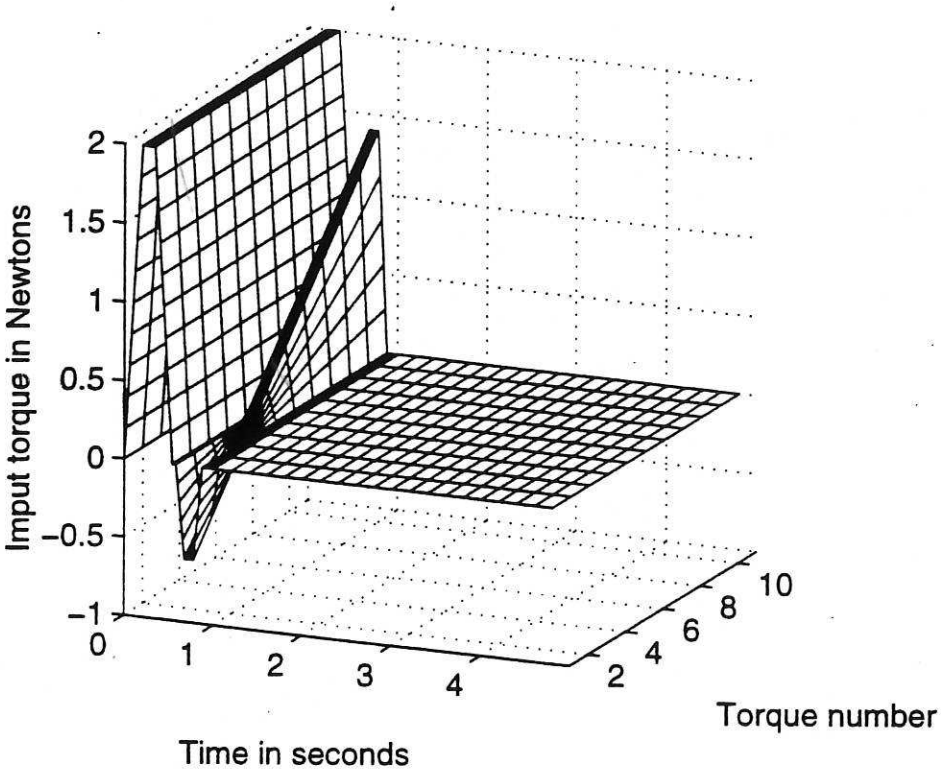

Figure 7(a). Input torque for the second link.

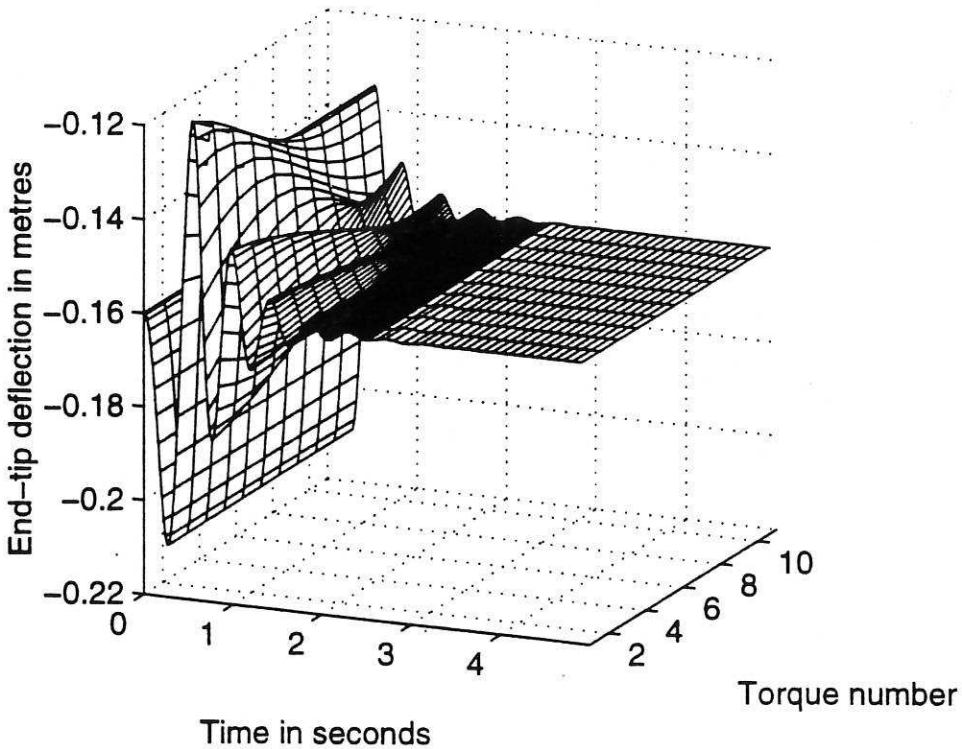

Figure 7(b). Response of the end–tip deflection of link 2.

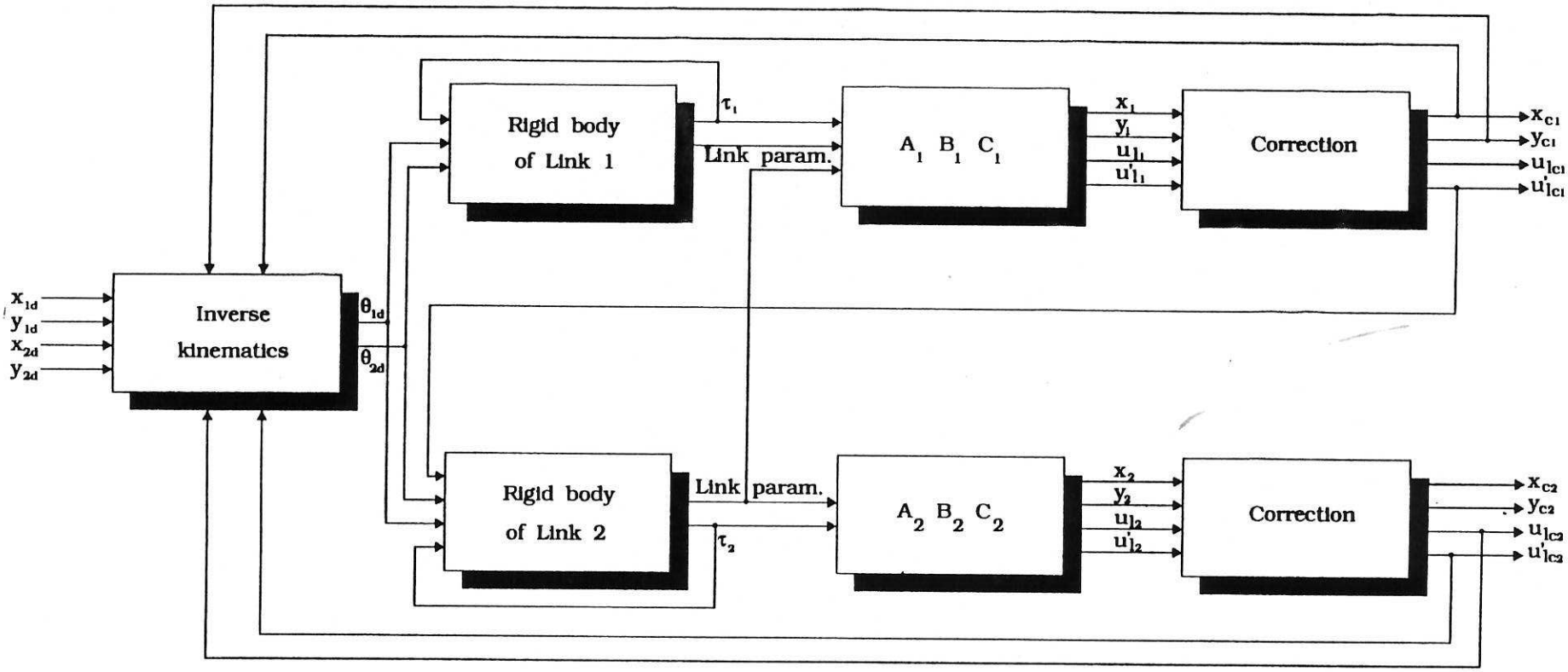

Figure 8. Block diagram of algorithm for modelling a two-link flexible manipulator.

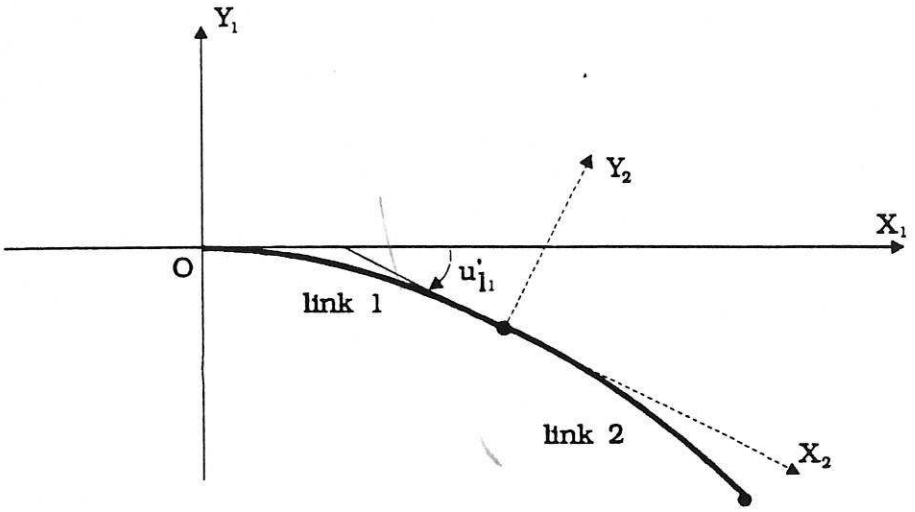

Figure 9(a). Initial conditions for the position of the manipulator. (the angles α are equal to 0)

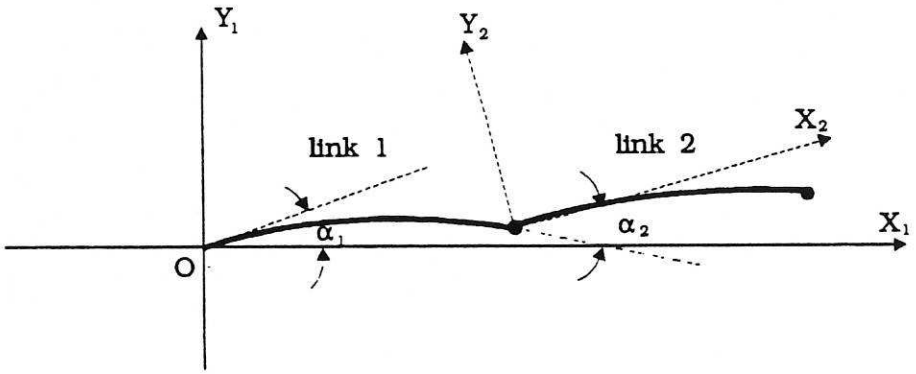

Figure 9(b). A different initial configuration of the manipulator showing the initial angles α_1 and α_2

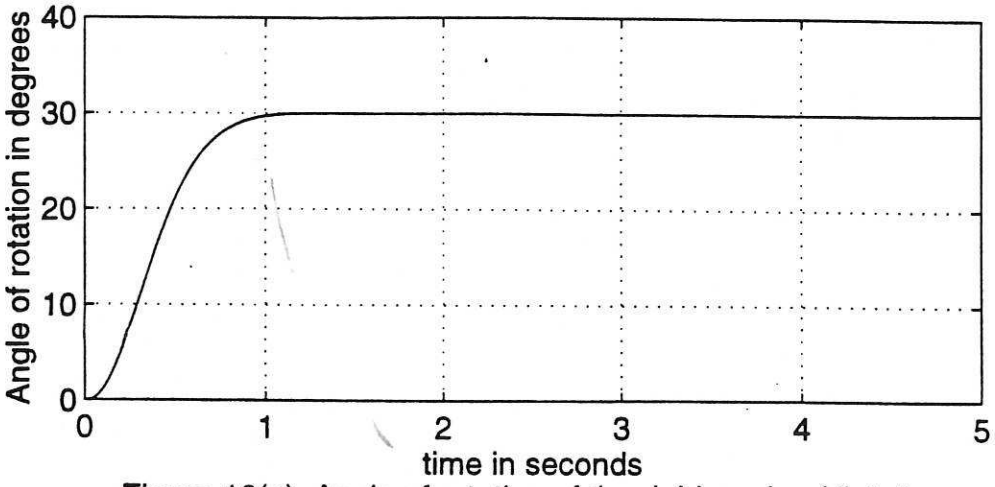

Figure 10(a). Angle of rotation of the rigid mode of link 1.

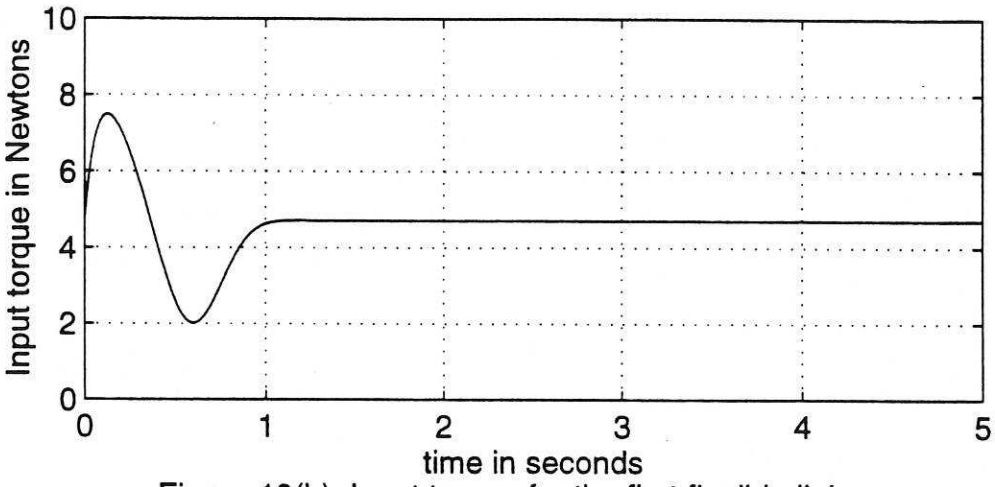

Figure 10(b). Input torque for the first flexible link.

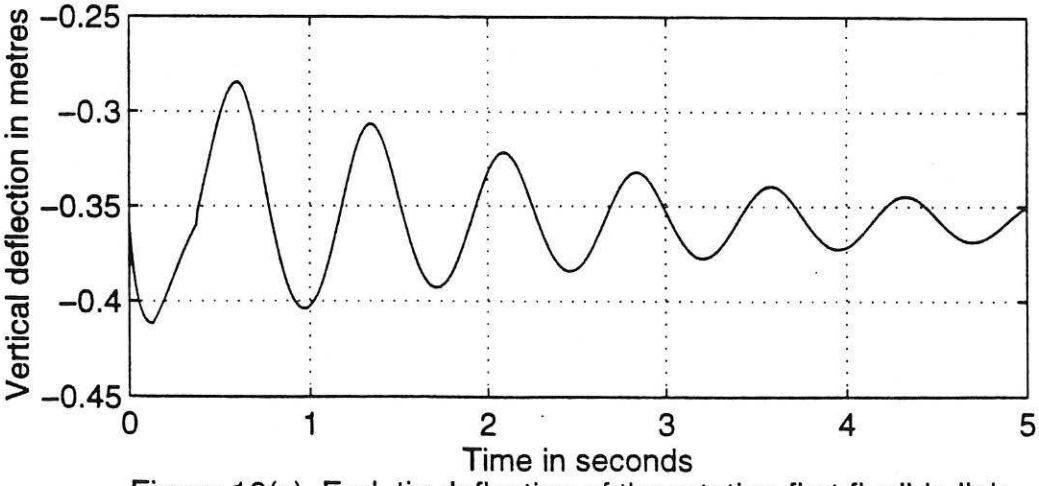

Figure 10(c). End–tip deflection of the rotating first flexible link.

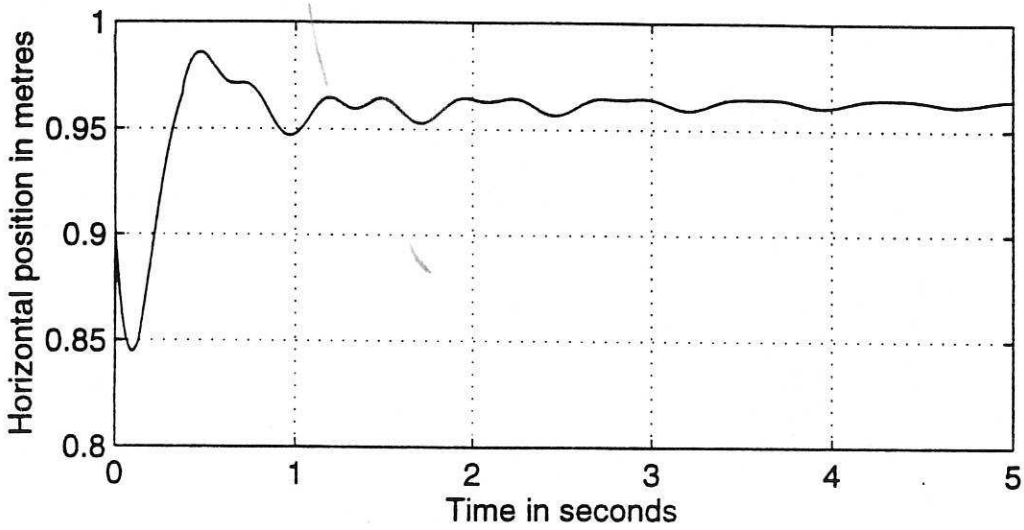

Figure 11(a). Horizontal position of the end–tip of the first link.

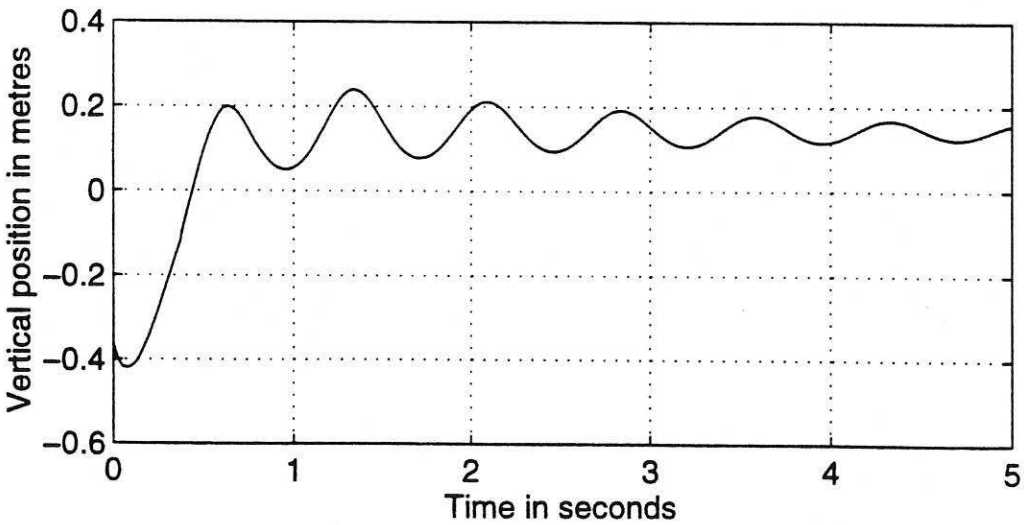

Figure 11(b). Vertical position of the end–tip of the first link.

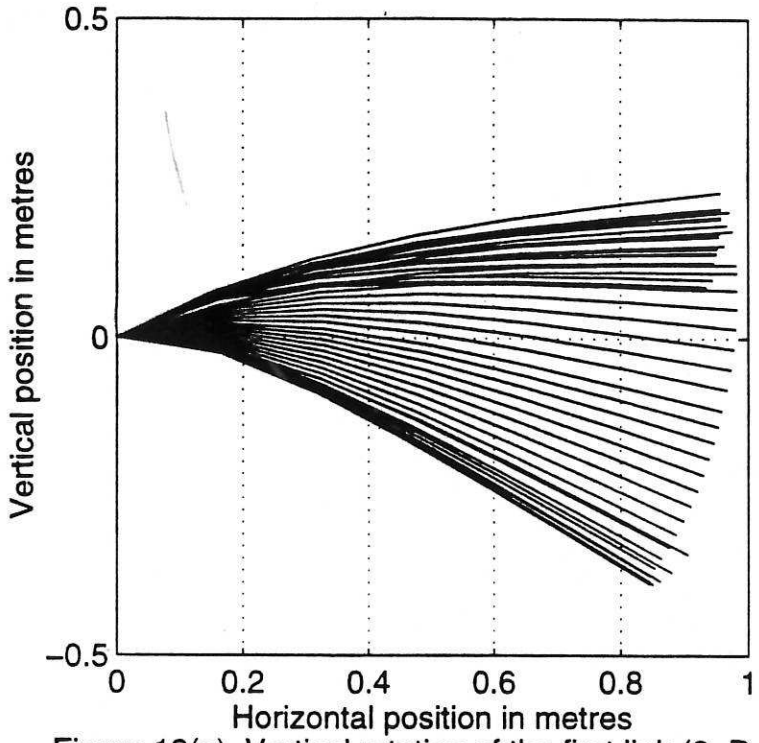

Figure 12(a). Vertical rotation of the first link (2–D view).

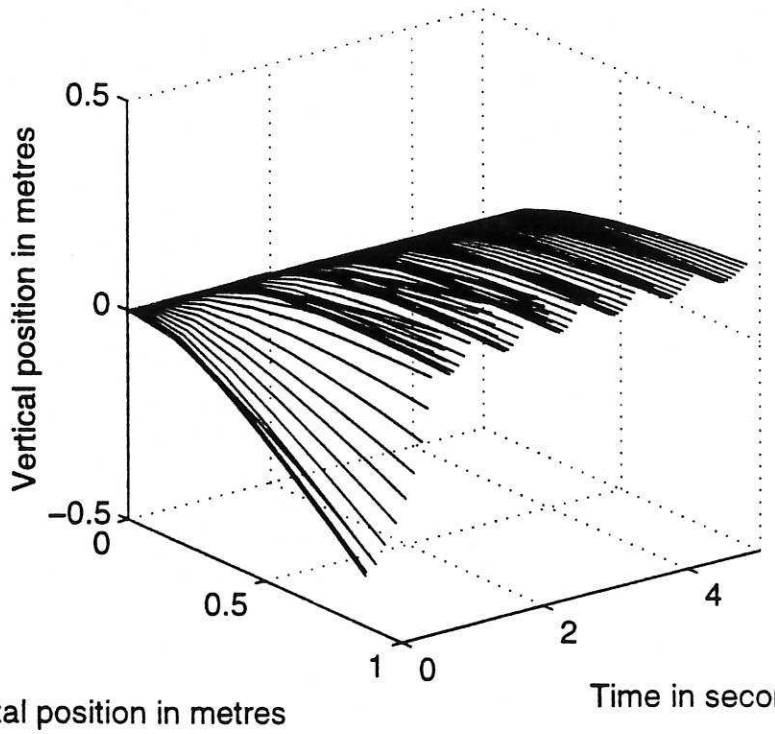

Figure 12(b). 30–degree rotation of the first flexible link (3–D view).

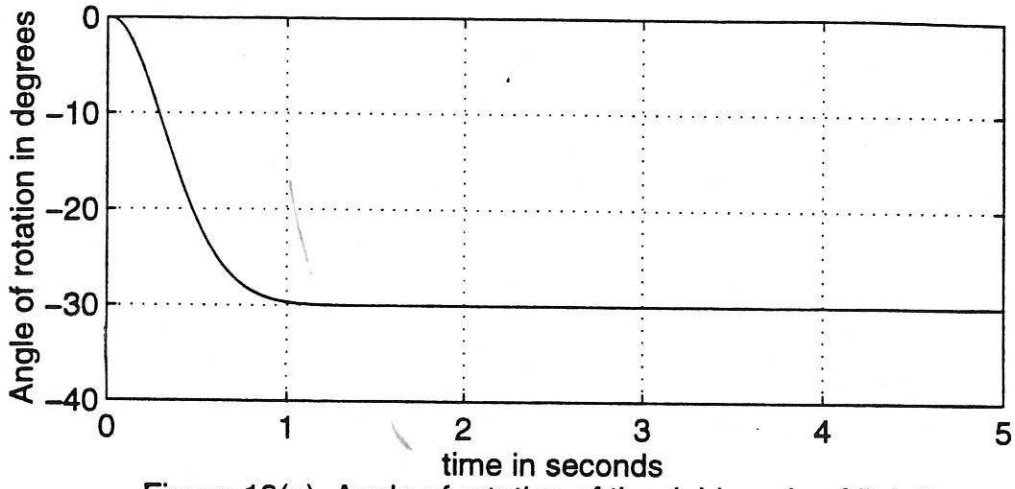

Figure 13(a). Angle of rotation of the rigid mode of link 2.

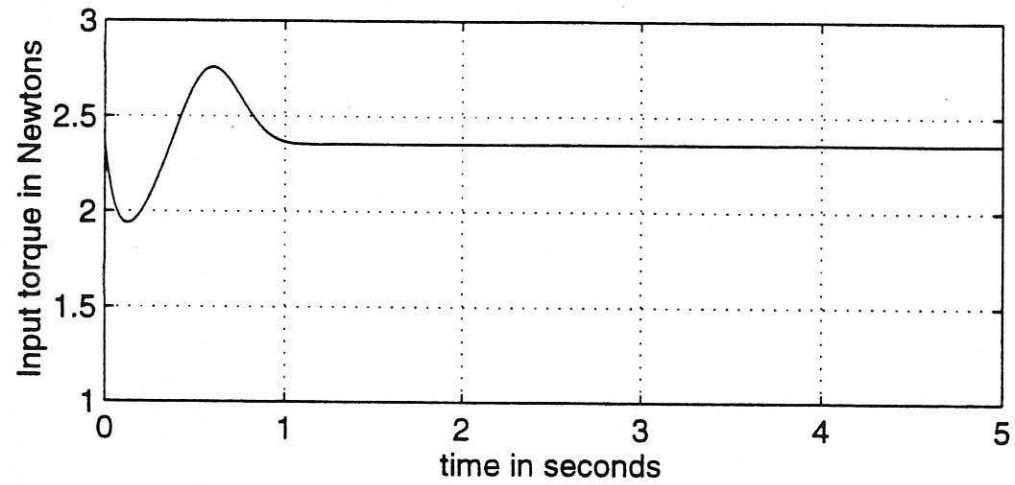

Figure 13(b). Input torque for the second flexible link.

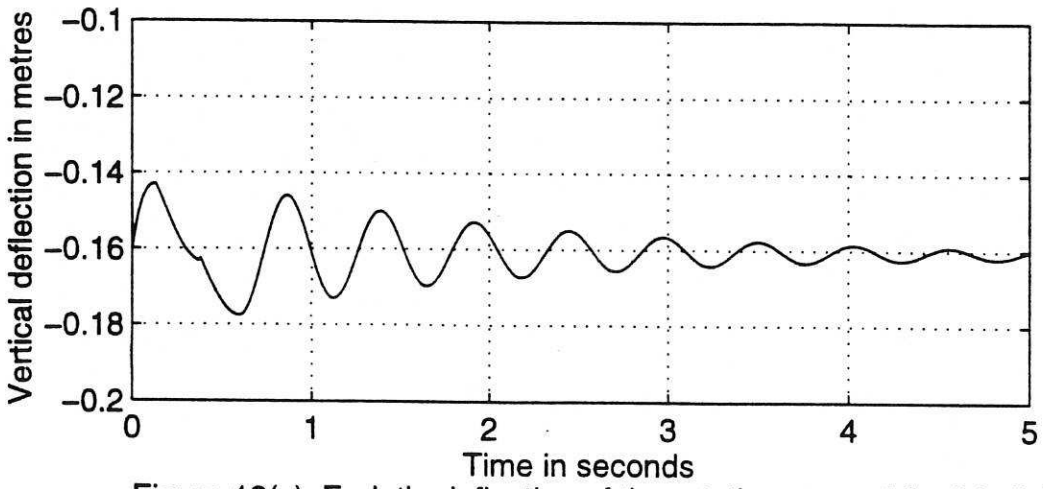

Figure 13(c). End–tip deflection of the rotating second flexible link.

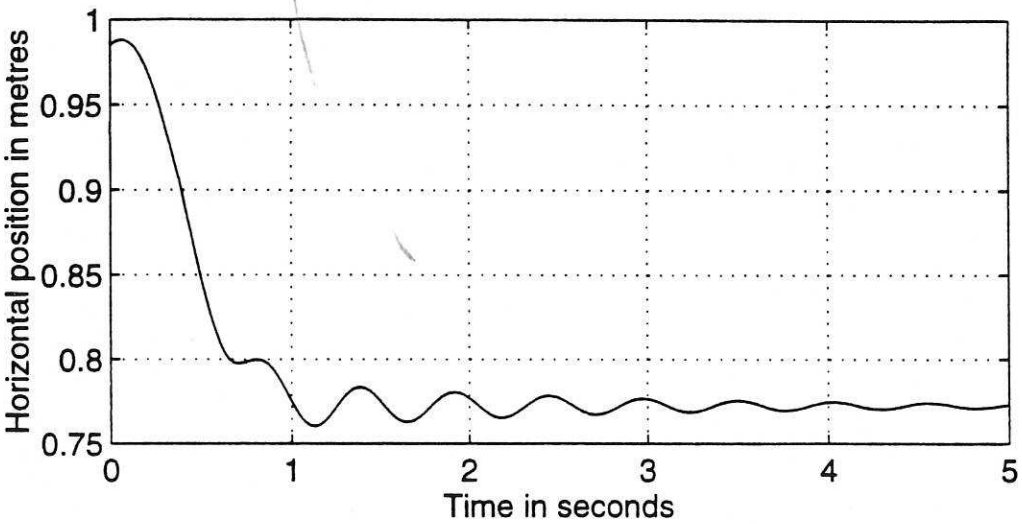

Figure 14(a). Horizontal position of the end–tip of the second link taken from the reference frame attached to this link.

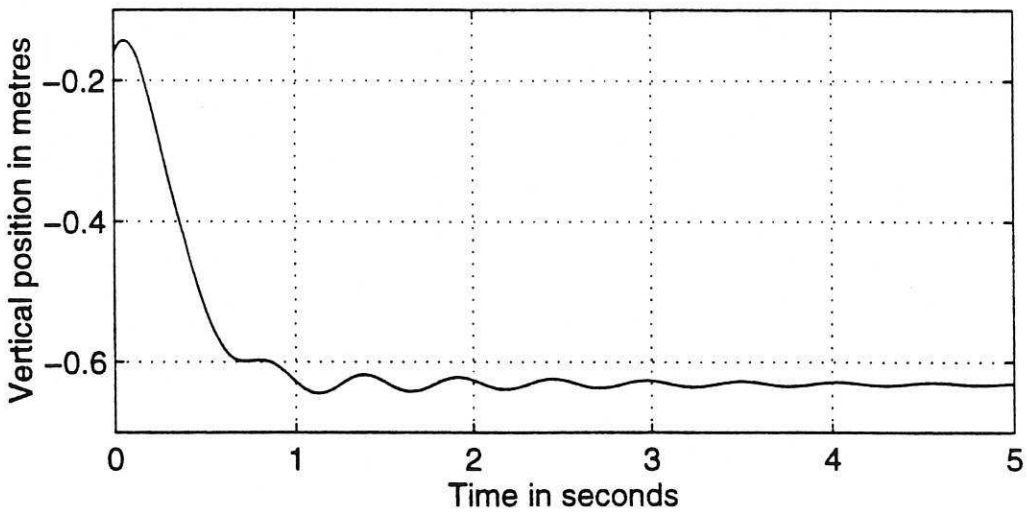

Figure 14(b). Vertical position of the end–tip of the second link taken from the reference frame attached to this link.

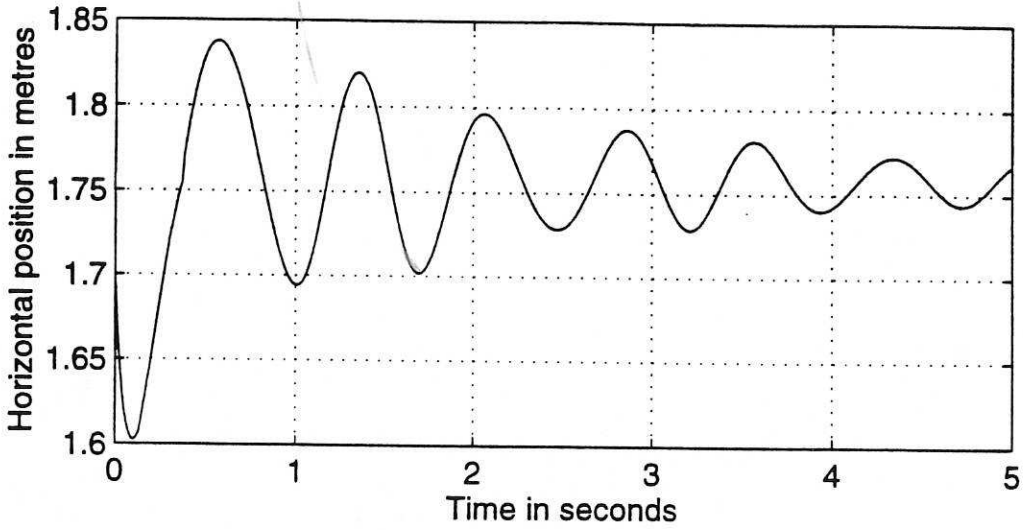

Figure 15(a). Horizontal position of the end–tip of the second link taken from the reference frame attached to link 1.

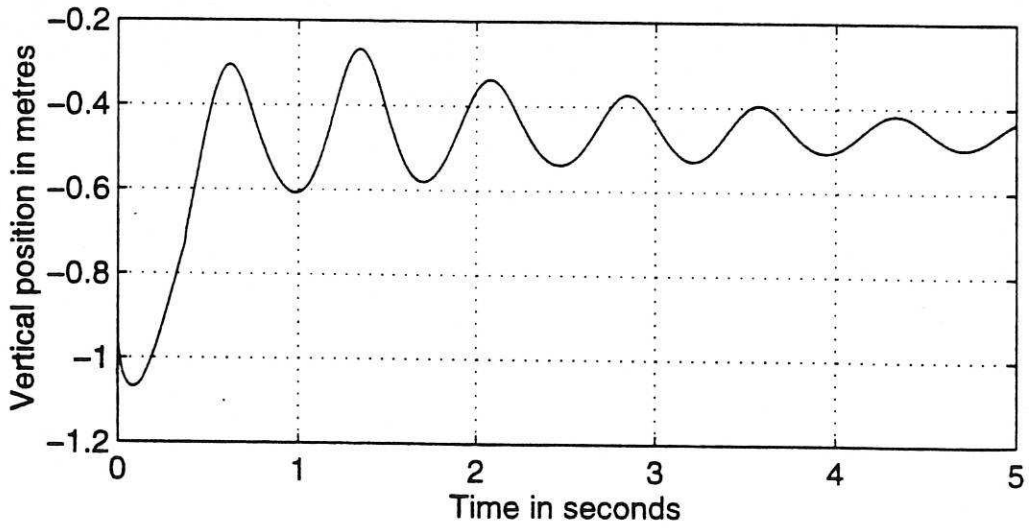

Figure 15(b). Vertical position of the end–tip of the second link taken from the reference frame attached to link 1.

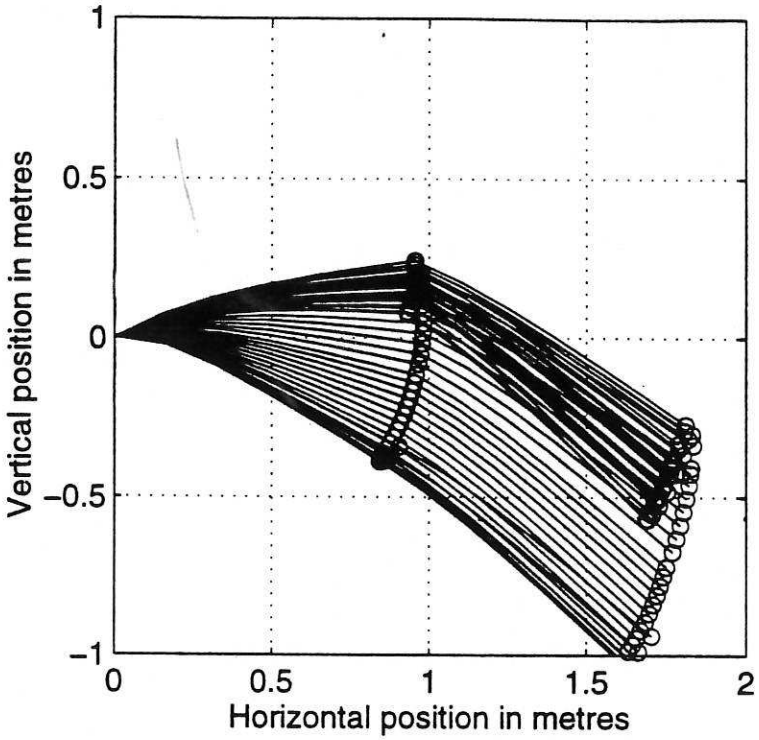

Figure 16(a). Vertical rotation* of the two links (2–D view).
* Theta 1 = +30 degrees. Theta 2 = –30 degrees.

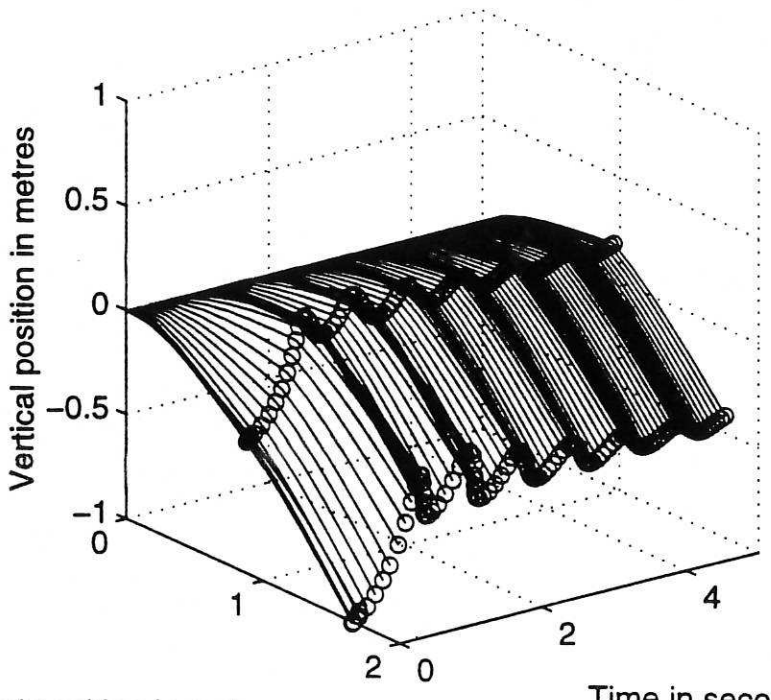

Figure 16(b). General motion* of the two flexible links (3–D view).